Metglas–Elgiloy bi-layer, stent cell resonators for wireless monitoring of viscosity and mass loading

Metglas–Elgiloy bi-layer, stent cell resonators for wireless monitoring of viscosity and mass loading

Anupam Viswanath[1]**, Scott R Green**[1]**, Jürgen Kosel**[2]
and Yogesh B Gianchandani[1]

[1] Department of Electrical Engineering and Computer Science and Center for Wireless Integrated MicroSensing and Systems (WIMS2), University of Michigan, Ann Arbor, MI, USA
[2] Computer, Electrical and Mathematical Sciences and Engineering Division, King Abdullah University of Science and Technology, 4700 KAUST, Thuwal 23955, Saudi Arabia

E-mail: anupamv@umich.edu

Abstract

This paper presents the design and evaluation of magnetoelastic sensors intended for wireless monitoring of tissue accumulation in peripheral artery stents. The sensors are fabricated from 28 μm thick foils of magnetoelastic 2826MB Metglas^{TM}, an amorphous Ni–Fe alloy. The sensor layer consists of a frame and an active resonator portion. The frame consists of 150 μm wide struts that are patterned in the same wishbone array pattern as a 12 mm $\times$ 1.46 mm Elgiloy stent cell. The active portion is a 10 mm long symmetric leaf shape and is anchored to the frame at mid length. The active portion nests within the stent cell, with a uniform gap separating the two. A gold-indium eutectic bonding process is used to bond Metglas^{TM} and Elgiloy foils, which are subsequently patterned to form bi-layer resonators. The response of the sensor to viscosity changes and mass loading that precede and accompany artery occlusion is tested *in vitro*. The typical sensitivity to viscosity of the fundamental, longitudinal resonant frequency at 361 kHz is 427 ppm cP^{-1} over a 1.1–8.6 cP range. The sensitivity to mass loading is typically between 63000 and 65000 ppm mg^{-1} with the resonant frequency showing a reduction of 8.1% for an applied mass that is 15% of the unloaded mass of the sensor. This is in good agreement with the theoretical response.

(Some figures may appear in colour only in the online journal)

1. Introduction

Stents are metal mesh tubular structures used to treat narrowed vessels and ducts in the body that have been constricted as a result of stenosis. Balloon angioplasty is an established procedure for the implantation of these stents. Although angioplasty relieves the symptoms of stenosis, it carries with it a risk of a reappearance of the narrowing, typically due to the reaction of the body to the presence of the stent—a condition known as in-stent restenosis.

Peripheral arterial disease (PAD) comprises those pathologies which result in obstruction to blood flow in the arteries, exclusive of the coronary and intracranial vessels. Although the definition of PAD technically includes problems within the extracranial carotid circulation, this work is directed at chronic arterial occlusive disease occurring in the legs. The most common cause of PAD is hardening of the arteries (atherosclerosis), the gradual buildup of fatty deposits (plaque) on the walls of the arteries that slow or block blood flow (figure 1). Plaque buildup also causes the artery walls to stiffen and become unresponsive to varying levels of blood supply. Intermittent claudication, defined as pain in the muscles of the leg with ambulation, is the earliest and the most frequent presenting symptom in patients with lower extremity PAD. Although claudication symptoms are typically localized in the calf or the thigh, 'rest pain' is characteristically in the foot [1]. In the late stages of PAD, tissue hypoperfusion progresses to ischaemic ulceration and gangrene, and major amputation is
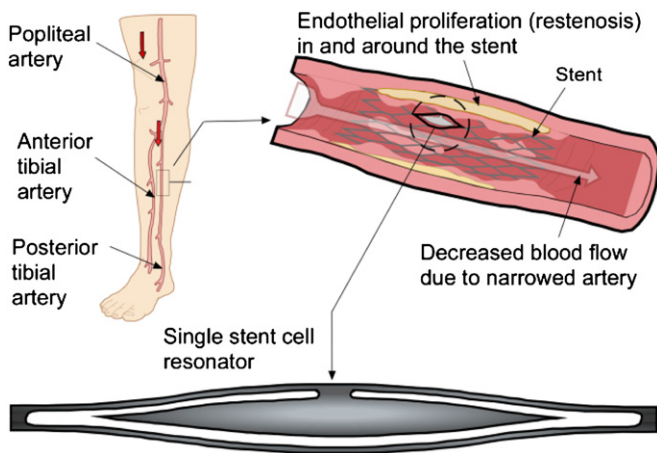
Figure 1. Conceptual diagram showing restenosis occurring in the posterior tibial artery and the integration of sensor on stent. A schematic of the Metglas™/Elgiloy single stent cell resonator used for sensing is also shown.

Figure 2. Conceptual diagram of magnetoelastic monitoring of peripheral stents located in the posterior tibial artery. External circuitry drives the external interrogation coils to wirelessly measure the response of the implanted sensor.

eventually required in more than a third of the patients. In most severe cases of PAD, surgical interventions such as angioplasty are necessary for treatment.

Once a stent is implanted, the patient is at risk for restenosis, a process in which the open lumen of the stent is occluded by hyperproliferation of endothelial cells. Various methods for the prevention of restenosis have been investigated. These methods include administering the patient with medications such as statin to reduce low-density lipoprotein cholesterol or clopidogrel to reduce risk for blood clots. Stents coated with a pharmacologic agent (drug eluting stents) are known to interfere with the process of restenosis. Since these methods do not assure the prevention of restenosis, the patient must be monitored to ensure patency of peripheral stents on a regular basis.

Current techniques for the diagnosis of PAD and restenosis in stented peripheral arteries include quantitative Doppler ultrasonographic measurements of blood flow velocity [2–4]. Duplex ultrasound has been used to define the anatomic extent of PAD. Although these methods have been useful in documenting the patency of a single arterial segment, such as a stented superficial femoral artery or a bypass graft, assessment of the entire lower extremity arterial tree remains imprecise and its adequacy as the sole diagnostic modality for planning a percutaneous or open surgical intervention remains controversial [5].

Magnetoelastic resonance angiography, as used in this work, serves as a direct method for the detection of blockages in stents and can thus enable timely medical intervention. The method is outlined in figure 2. A magnetoelastic sensor integrated with the stent resonates at a frequency that responds to changes in mass loading, and to a lesser extent to changes in the blood viscosity. The mechanical resonance is interrogated by a set of external coils. The transmit, pickup and dc magnetic coils are placed in a co-axial coil configuration in a sleeve around the limb. This interrogation technique utilizes magnetic inductive coupling for a short interrogating distance (near field). Unlike other purely electromagnetic wireless techniques, magnetoelastic coupling exploits the relationship
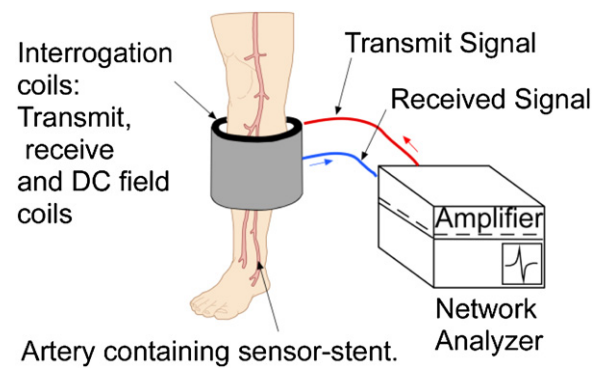
between magnetization response to a magnetic field and the strain of the sensor material. There are at least two important advantages of this method over purely electromagnetic methods. Firstly, magnetoelastic materials have high coupling coefficients and high magnetic permeability, negating the need for an internal antenna within the stent geometry. This is valuable in this space-limited application. Secondly, because the typical resonant frequency of these sensors can be designed to lie within a range of <400 KHz, the attenuation posed by bodily tissue when interrogating the sensors is low. Antennas of sizes similar to the sensors used in this work have working frequencies in the 0.1–1 GHz range. Bodily tissue has much higher attenuating properties at those frequencies.

Our previous work demonstrated magnetoelastic sensors incorporated with stents for sludge accumulation in a biliary stent [6–8]. Initial designs were tethered to the stents with anchors, separating sensor and the stent [6]. Although a reasonable architecture for biliary stents, this separation could lead to problems such as undesirable blood turbulence and blood clotting in peripheral stents [9]. A closer integration of the sensor with the stent to form a bi-layer resonator would help reduce clotting potential. A sensor design is needed that permits better conformity to the expanding stent structure, while still providing adequate sensitivity. An effective bonding method for sensor-stent integration is also needed.

Magnetoelastic resonant sensing has attracted considerable interest in the sensor community as the method can be used to measure a wide variety of environmental parameters including pressure [10], humidity [11], temperature [12] and liquid viscosity [13]. These sensors have the relative advantages of immunity to noise and changes in the amplitude or orientation of the interrogation field. Another important advantage of these sensors in the context of implantable devices is the ability to be wirelessly interrogated. This paper presents a sensor integrated with a stent for wirelessly monitoring the restenosis in a peripheral artery stents. The design, modeling and material selection for the sensors are described in section 2 followed by the fabrication approach in section 3 and experimental results in section 4. The discussions and conclusions are presented in section 5.

Table 1. As-cast material properties of Metglas^{TM} 2826 MB alloy.

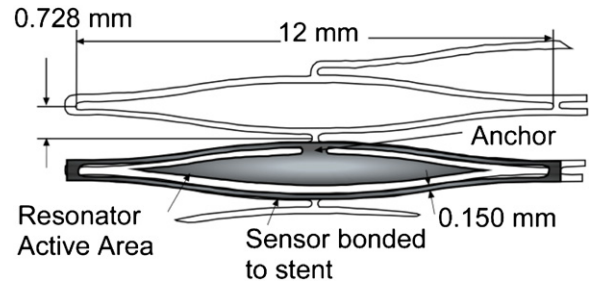|	
Density (kg m^{-3})	7900
Thickness (μm)	28
Saturation magnetostriction (ppm)	12
Saturation bias field (Oe)	8

2. Design and modeling

2.1. Material selection for the resonant sensors

Magnetoelastic sensors are typically made of amorphous ferromagnetic ribbons or wires, mostly iron-rich alloys such as $Fe_{40}Ni_{38}Mo_4B_{18}$ (brand name Metglas^{TM} 2826MB), $Fe_{90}Si_5B_5$ (brand name Metglas^{TM} 2605SA1) and $Fe_{67}Co_{18}B_{14}Si_1$ (brand name Metglas^{TM} 2826CO) [14, 15]. The Metglas^{TM} ribbons listed above have a high magnetoelastic coupling coefficient, as high as 0.98, and magnetostriction on the order of 10^{-5} [16–18]. A high magnetoelastic coupling allows efficient conversion between magnetic and elastic energies and vice versa. In addition, the magnetomechanical coupling coefficient of the sensor can be controlled by annealing the magnetoelastic material in a transverse magnetic field [19–25], or changing the bias field and/or sensor aspect ratio.

In our previous work we studied the properties of each of the Metglas^{TM} alloys (2826MB, 2605SA1 and 2605CO) with simple sensor designs [7]. Along with maintaining a usable wireless signal under loading, the sensor must present a low profile (to maintain the open flow channel of the stent) and must not hinder the mechanical operation of the stent (especially expandability and bending flexibility). The amorphous alloys mentioned above can meet these requirements, as they are thin ($\approx$25 μm), can be located along the sidewall of the stent and can also be patterned such that the sensor expandability matches that of the stent.

In an effort to improve the elasticity of the stent, chrome-nickel Elgiloy is used. Elgiloy is advantageous in the sense that it has a much higher yield strain than stainless steel: $\approx$1% for Elgiloy versus $\approx$0.15% for 316 L stainless steel [26]. Elgiloy is also less prone to corrosion. In order for the sensor to conform better to the stent, a sensor material would have to possess appropriate elastic properties. Fortunately, Metglas^{TM} alloys meet the requirements for both magnetostrictive and elastic properties. For instance, the 2826MB alloy, as used in this effort, is reported to have a yield strain of 1.6%, which is even higher than that of cold-reduced Elgiloy [27]. Some important material properties of Metglas^{TM} 2826MB alloy are listed in table 1.

2.2. Structural design

As shown in figure 3, the sensor design conforms to the cell of a conventional stent structure. The stent design follows a wishbone-array pattern that is favored for its flexibility during expansion. A similar pattern is used in commercial stents such as the PRECISE® PRO RX® and the CYPHER® (Cordis Corporation, a Johnson and Johnson company). The bonding of magnetoelastic material to stent material is followed by

Figure 3. Sensor and stent geometry showing important dimensions. A sensor bonded to a single stent cell is also shown.

patterning into the shape of conventional stent cells with overhanging bi-layer resonators formed at particular locations along the stent. The bonding strategy used for this integration is described in section 3. The dimensions of the stent cell and the sensor active area are shown in figure 3. The sensor layer comprises a frame and an active resonator portion. The frame consists of 150 μm wide struts that are patterned in the same wishbone-array pattern as a 12 mm × 1.46 mm stent cell. The frame is bonded to the stent struts. The active portion is a 10 mm long symmetric leaf shape and is connected to the frame with a small anchor at mid-length. The leaf shape nests within the frame and stent cell, with a uniform gap separating the active portion from the frame. This gap is 125 μm wide and allows for mechanical decoupling between the sensor and the frame. The typical active area of a sensor is approximately 4.5 mm². The resonator is excited in its fundamental, longitudinal extensional mode of vibration which produces movement of the ends of the active area of the sensor.

The stent application calls for a generally tubular shape for use in angioplasty. This sensor design allows for the easy coiling of stents into this shape without excessive mechanical strain on the magnetoelastic material, which may lead to unwanted shifts in resonance response.

2.3. Modeling

The magnetomechanically coupled finite element analysis (FEA) tool presented in [6] is used to estimate frequency responses and expected signal amplitudes of the sensors. The desired sensor geometry is modeled in the FEA program, along with the geometry of the transmit and receive coils. In the simulations, the transmit and receive coils have an internal diameter of 14 and 13 cm respectively. The sensor is positioned along the central axis of the transmit/receive coils with a radial distance of 6.5 cm separating the sensor from the receive coil. The current in the transmit coil was measured and applied in the model to generate the field at the sensor. The magnetic flux density emanating from the sensor was integrated numerically (with appropriate scaling factors) over the volume of the receive coil to calculate the induced EMF. The apparent modulus, permeability and magnetostrictivity used in the model were based on available literature values. These values were modified slightly to improve the fit with experimental frequency responses obtained from stent cell resonators fabricated from the actual material used. A baseline
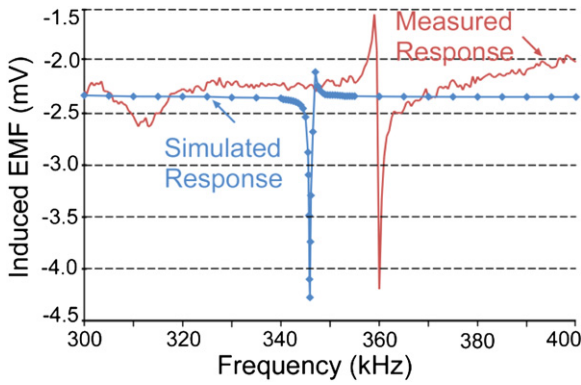
Figure 4. Frequency response of unloaded sensor in air. The measured resonant frequency is 361 kHz while the custom magnetomechanical FEA model resonates at 346 kHz.
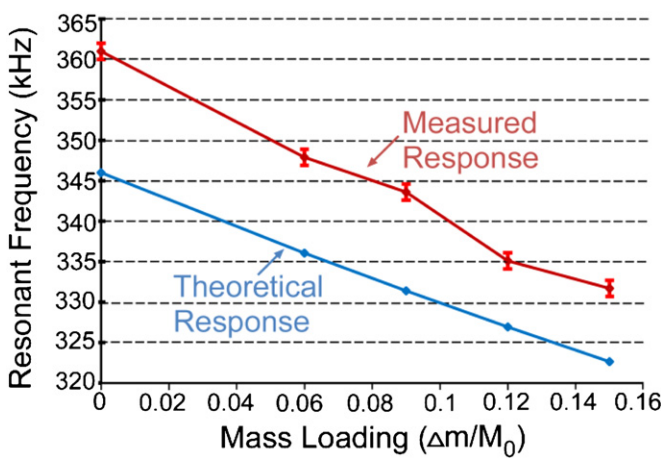

Figure 5. Stent cell resonator response to mass loading in water flow (velocity of 15 cm s^{-1}) and at a temperature of 37°C. Mass loading is provided by paraffin wax. M_o denotes the unloaded sensor mass and Δm the mass load on the sensor.

Figure 6. Process flow for the fabrication of bi-layer stent cell resonators integrated with the stent. (1) Metglas^{TM} 2826MB and Elgiloy foils are aligned and bonded using the Au–In eutectic bonding process to form the bi-layer. (2) Batch patterning of the bonded foils is performed using μ-EDM. (3) Bi-layer stent cell resonators at specific locations along the stent frame are fabricated. Parylene deposition is then performed on the resonators to passivate them and make them bio-compatible.

signal was taken in the absence of the sensor, which was simulated by setting the magnetoelastic coupling coefficient to zero. This baseline was subtracted from the overall signal, with the sensor present. Figure 4 shows the simulated frequency response of the sensor. The simulated resonant frequency for the stent cell resonators in its fundamental longitudinal mode of vibration is 346 kHz. The simulated response has a signal amplitude of 2.3 mV at resonance. In addition, the theoretical response of magnetoelastic sensors to uniform mass loading is given by the following characteristic equation [14]:

$$f_{\text{loaded}} = f_{o,\text{unloaded}} \sqrt{\frac{1}{1 + \left(\frac{\Delta m}{M_o}\right)}}. \tag{1}$$

In this equation, f_{loaded} and $f_{o,\text{unloaded}}$ denotes the mass loaded and unloaded resonant frequencies of the sensor respectively. M_o denotes the un-loaded mass of the sensor and Δm denotes the mass load on the sensor. The simulated frequency response of the sensor to mass loads is shown in figure 5. The FEA simulated, unloaded resonant frequency of 346 KHz is used in the analytical model.
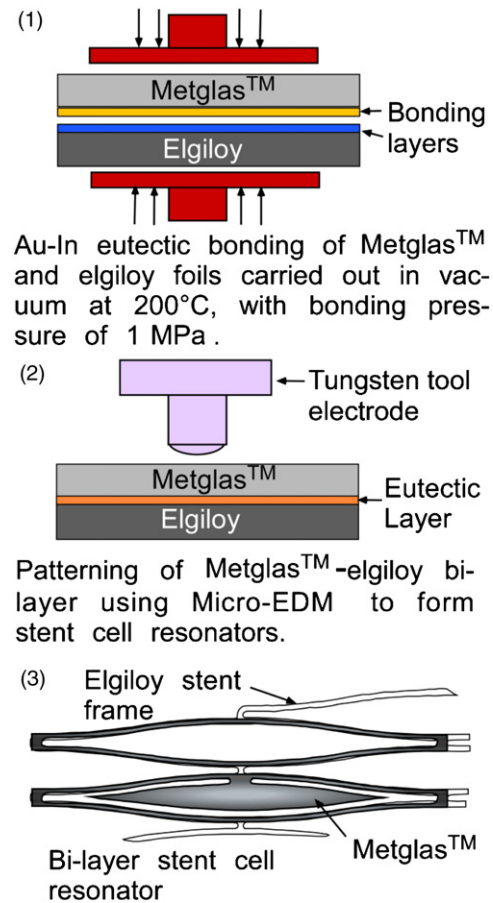
3. Fabrication

The process flow for the fabrication of bi-layer stent cell resonators integrated with the stent is shown in figure 6 (this process is intended to provide rapid prototyping for research investigations and will need to be modified for final production). Metglas^{TM} 2826 MB and Elgiloy foils are aligned and bonded using the Au–In eutectic bonding process. This results in bi-layer foils comprising the sensor and stent material. Batch patterning of the bonded foils is then performed using μ-EDM (micro-electrode discharge machining) to result in bi-layer stent cell resonators at specific locations along the stent frame.

A number of bonding techniques were evaluated to integrate Metglas^{TM} 2826MB onto the Elgiloy stent material. These include methods such as parylene–parylene bonding, dental cements, hot-plate and Nanofoil^{TM} soldering. The most successful technique was the gold–indium (Au–In) eutectic bond [28]. This process involves the deposition of multiple layers of Au and In on the component metal surfaces. A low temperature bonding process is carried out between the
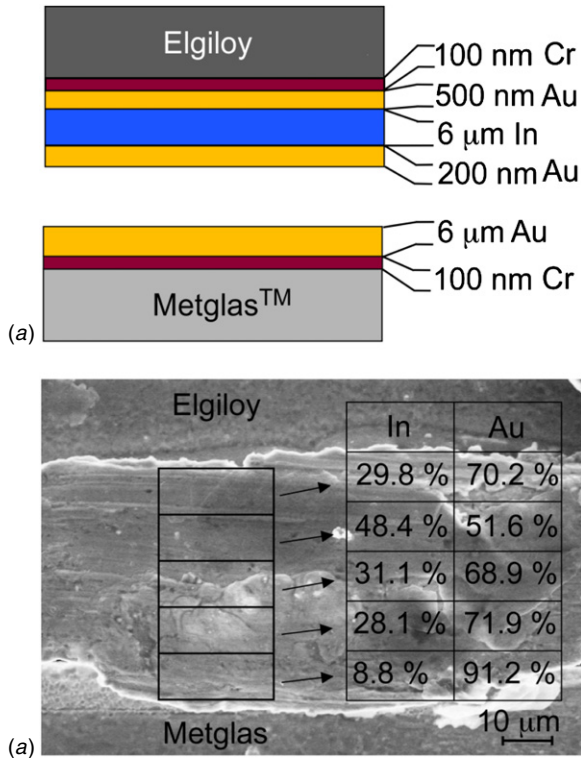
Table 2. Bonding process parameters.

Bonding temperature	200°C
Bonding time	60 mins
Heating ramp rate	10°C min^{-1}
Cooling ramp rate	1.65°C min^{-1}
Bonding pressure	≈0.95 MPa
Vacuum pressure	29.4 mTorr

Figure 7. (*a*) Initial deposited layer thicknesses prior to Au–In eutectic bonding. (*b*) SEM image of bond cross-section showing Au–In eutectic alloy formation. EDX analysis was performed to show weight percentages of gold and indium across the bond.

two components up to 200 °C. Above 157 °C the indium layer melts and dissolves the gold layers to form a mixture of liquid and solid. The solid-liquid interdiffusion process continues until the mixture solidifies to form the Au–In bond. This technique has established high bond strengths ranging from 4.4–10 MPa in literature, and is a relatively low temperature process having a high bond re-melting temperature [29]. The low temperature process is beneficial in avoiding thermal stresses induced in the magnetoelastic material that may otherwise lead to recrystallization or shifts in performance.

The final fabrication sequence is as follows: Elgiloy foils (125 μm thick) are first subjected to a back-sputtering treatment to improve Cr/Au adhesion to its surface. This involves plasma treatment of the Elgiloy at a power of 150 W in oxygen gas flow for a time period of 60 s. Subsequent chrome deposition then results in chrome oxide formations leading to better adhesion, which were confirmed by simple scotch tape peel tests. The Elgiloy foils are then pre-coated with a 0.6 μm thick Cr/Au adhesion layer (using an evaporation technique) and a 6 μm thick indium layer (using electroplating). As an added precaution, a 0.2 μm thick Au layer helps prevent oxidation of indium prior to bonding. The 28 μm thick Metglas^{TM} foil surfaces are coated with a 100 nm Cr adhesion layer (using evaporation technique) and a 6 μm gold layer (using an electroplating technique). These make up the eutectic ingredient layers on the metal surfaces required for the bonding process. A schematic of the bonding layer thicknesses is shown in figure 7(*a*). Thicknesses of electroplated/sputtered gold and indium are chosen to result in specific weight percentages of

27% In and 73% Au in the final eutectic bond. This particular stoichiometry allows for a low temperature formation of the eutectic at 200 °C while having a high re-melting temperature of 450 °C [28]. The minimum allowable thicknesses of bonding layers were set in order to overcome the maximum surface roughness of metals. The surface roughness of both metals is measured using an Olympus LEXT Interferometer. The maximum peak-to-peak variation of surface roughness is measured to be ≈6 μm for Metglas^{TM} 2826MB and 3 μm for Elgiloy. The bonding layers thicknesses chosen (figure 7(*a*)) add up to 12.9 μm and hence overcome the inherent surface roughness of the component metals.

The Au–In eutectic bonding process is performed in a vacuum oven at a temperature of 200 °C, with 1 MPa pressure applied. Bonding pressure is applied using custom designed, spring-loaded C-clamps which are calibrated for pressure loading. Glass slides are used to uniformly distribute pressure along the area of the bonding materials. A heating ramp rate of 10 °C min^{-1} and a cooling rate of 1.65 °C min^{-1} ensure adequate inter-diffusion and solidification of the mixture to form the Au–In bond. Table 2 lists the parameters used in the bonding process. The Au–In eutectic bonding allows for a bonding layer that is ≈12.9 μm thick. Combining the 28 μm thick Metglas^{TM} and 150 μm thick Elgiloy foils, this results in a total thickness of ≈190 μm for the bi-layer. Figure 7(*b*) shows an SEM image of a test structure that has been sectioned by μEDM after bonding. EDX analysis was performed to show weight percentages of gold and indium across the bond.

Isolated, single stent cell resonators are patterned from a pre-bonded Metglas^{TM} 2826MB to Elgiloy piece. Batch patterning of these resonators is carried out by serial μEDM of pre-bonded Metglas^{TM} to Elgiloy pieces. Tungsten tool electrodes of 125 μm diameter provide a good compromise between machining speed and minimum feature sizes achievable and were thus used in the μEDM process. The machined sensors are released and cleaned thoroughly to remove any debris as a result of the machining. The resulting single stent cell resonators are bi-layers of Metglas^{TM} 2826MB and Elgiloy. A fabricated, isolated, single stent-cell, bi-layer resonator is shown in figure 8.

Magnetoelastic alloys are known to corrode in aqueous environments due to its high iron content. To passivate the material, the sensors are coated in a conformal layer of 200 nm thick Parylene-C using a standard vacuum deposition technique. This process results in sensors that are more robust in corrosive environments while causing negligible shifts in resonator frequency and amplitude response.
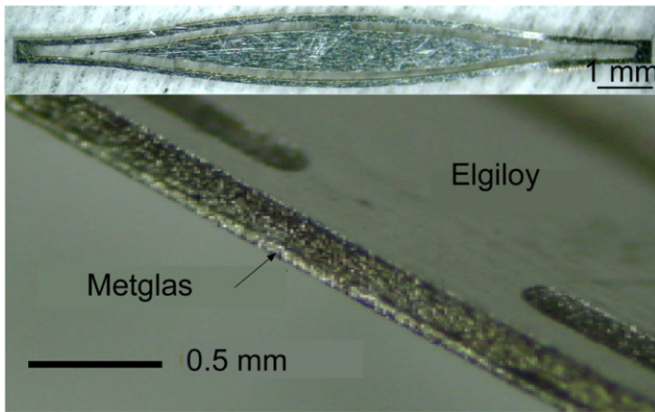
Figure 8. Fabricated resonators (*a*) Isolated sensor comprising of bi-layer Metglas™–Elgiloy resonators. (*b*) Perspective view of the anchor of the bi-layer resonators.
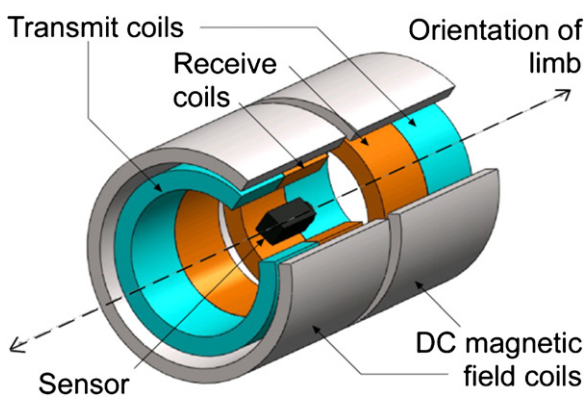

Figure 9. Co-axial coil configuration used for resonance measurements during *in vitr*o tests.

4. Experimental methods and results

A co-axial coil configuration was used for benchtop testing and evaluation of the sensors (figure 9). Dual-Helmholtz coils were used to provide a uniform and well-controlled dc bias field to the sensors. The dc magnetic bias was used to set the operating point of the sensor response [6–8]. The transmit coils were located on both sides of the receive coils. The transmit and receive coils were aligned in a co-axial and concentric configuration within the DC bias field coils. The inner diameter of all coils was chosen to be 13 cm. The number of turns in the dual-layered transmit and receive coils were chosen to be 48; the dc coils were wound with 102 turns. Wires of 22 AWG type were used in the coils.

The sensor to be evaluated was positioned at the center of this co-axial coil configuration, with the long axis of the sensor oriented along the coil axis. The transmit and receive coils were driven and measured by an Agilent 4395A network analyzer. The output signal from the network analyzer was amplified using a power amplifier (Model 7500, Krohn-Hite Corporation, Massachusetts, USA). The dc coils were powered by a 6.2 V, 4.2 A signal from a dc power supply. A Hall probe (AD22151, Analog Devices, Inc.) was used to measure the resulting magnetic bias field strength across the sensor.

This measurement setup is consistent with the configuration needed for an implanted sensor in one of the posterior arteries (i.e. arteries in the legs or hands) of the patient. Additionally, the co-axial coil configuration achieves a higher signal-to-noise ratio than other configurations and does not have stringent requirements for magnetoelastic sensor positioning within the coil [6].

Flow tests were performed using either a positive-displacement, dc-operated pump (B&D Mfg., Inc.) or a peristaltic pump, depending on the liquid flowing from the reservoir. Tubes having an inner diameter of 4.0 mm were used in the flow setup to mimic the average diameter of the posterior tibial artery [30]. The sensor was placed in the tube at the center of the interrogation coils. The temperature of the test liquid was maintained at 37 °C (mimicking normal human body temperature). Polyimide thermofoil heaters (Minco Products, Inc., Minnesota, USA) were placed on the outside of the tube to maintain a local temperature of 37 °C around the sensor.

Water has an average density that is close to that of blood and was consequently used in flow velocity sensitivity and mass loading tests. Evaluation of viscosity sensitivity involved the use of varying concentrations of sugar water solutions to mimic conditions of blood flow before and after restenosis. The sensitivity to flow velocity changes was evaluated by varying the power supply to the dc pump and hence the velocity of water. The velocities were varied between 20 and 11 cm s^{-1} to replicate conditions of blood flow in peripheral arteries during diastolic and systolic cycles respectively [31]. As viscosity changes of blood flow accompany the constriction leading to restenosis in an artery, the sensitivity to viscosity change was evaluated. Viscosity levels of the test liquid were varied between 1.1 and 15 cP using varying concentrations of sugar (sucrose) water solutions [32]. The velocity of flow for the sugar solutions was 15 cm s^{-1}. The volume of water used for each sample was 200 mL and the molar mass of sugar used in the calculations was 342.3 g mol^{-1}.

The sensitivity to mass loading was evaluated by application of paraffin wax onto the overhanging resonator portion of the sensor. The mass loaded sensors were subjected to water flow (velocity of 15 cm s^{-1}) at room temperature. A precise weighing scale (with 0.1 mg resolution) was used to measure the unloaded and loaded sensor mass. A repeatability assessment of the sensors was performed in water flow. The frequency response of the sensors was measured 15 times with a time interval of 10 min between successive measurements. The amplitude of the resonant peak (V_{res}) and the anti-resonant peak (V_{anti_res}) were measured, and the average of the two magnitudes was calculated. In all experiments the fundamental longitudinal mode of resonance was studied, unless otherwise noted.

The effect of the bonding process on the magnetic properties of magnetoelastic Metglas 2826MB™ material was assessed. The magnetic properties of the Metglas 2826MB™ material were studied using a vibrating sample magnetometer (VSM), (Princeton Corp., New Jersey, USA). Two sets of samples were tested: 'as-cast' ribbons and ribbons subjected to temperatures and pressures encountered in the bonding process (table 2). The magnetization curves for these two sets
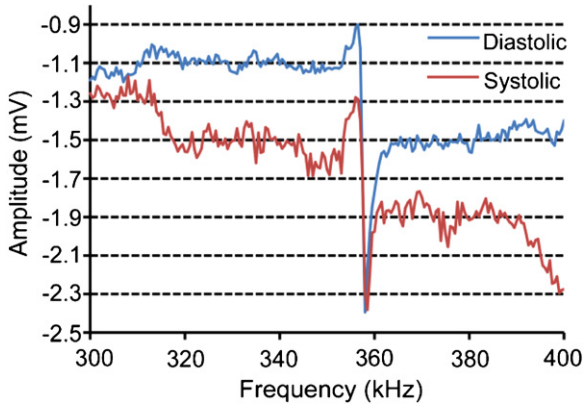
Figure 10. Measured resonance plots of bi-layer resonators in flow at 37 °C. Diastolic (flow velocity of 20 cm s^{-1}) observed f_{res} = 356.5 kHz while systolic (flow velocity of 11cm s^{-1}) observed f_{res} = 356.6 kHz.

Table 3. Magnetic properties of Metglas2826MB^{TM} ribbons in "as-cast" condition and ribbons subjected to bonding process temperature and pressure.

Metglas2826MB^{TM} ribbon type	Coercivity (mOe)	Remanence (memu)
"As-cast" ribbon	37.33	0.330
Exposed to bonding process	−142.6	−3.671

of samples were measured with the VSM. The magnitude of coercivity increased from 37.33 to 142.6 mOe. The measured magnitude of remanence also increased from 0.330 to 3.671 memu (table 3). Although there is slight increase in the magnitude of the coercivity and remanence, it is evident that the material remains magnetically soft and the practical effects on the sensor are insignificant.

Isolated sensors were tested *in vitro* for resonance response to various parameter changes. The unloaded response of a typical sensor in air is presented in figure 4. For this device, the typical unloaded resonant frequency is 361 kHz for the fundamental, longitudinal mode of vibration. The sensitivity was evaluated for changes in flow velocity of water. The flow velocity was varied between 20 and 11 cm s^{-1} to mimic systolic and diastolic conditions of blood flow. The measured frequency response for each condition, at 37 °C, is shown in figure 10. The maximum increase in resonant frequency, due to 9 cm s^{-1} decrease in flow velocity, fell within the measurement error of the network analyzer. The measured sensitivity of the fabricated sensors to flow velocity was less than 155 ppm cm s^{-1}. This is a favorable attribute because the sensors are not intended to respond to flow velocity.

The typical viscosity sensitivity of the sensors to varying viscosity levels of sugar water flow is presented in figure 11. The resonant frequencies measured are normalized to the unloaded, sensor resonant frequency in air. For viscosity levels of 1.084 and 8.596 cP, the measured resonant frequency was 357.65 and 356.505 kHz respectively. The maximum change in frequency observed is 0.32% over a 1.1–8.6 cP range. This corresponds to a viscosity sensitivity of 427 ppm cP^{-1} for the sensor.
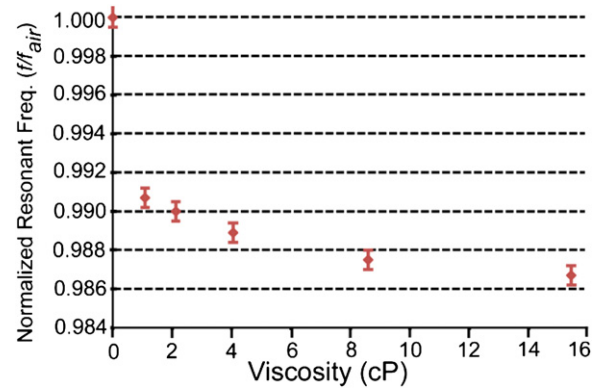

Figure 11. Stent cell resonator response to changes in viscosity levels. Viscosity is varied from 1.1 to 15.4 cP using varying concentrations of sugar (sucrose) in water. The resonant frequencies measured are normalized to the unloaded, sensor resonant frequency in air.
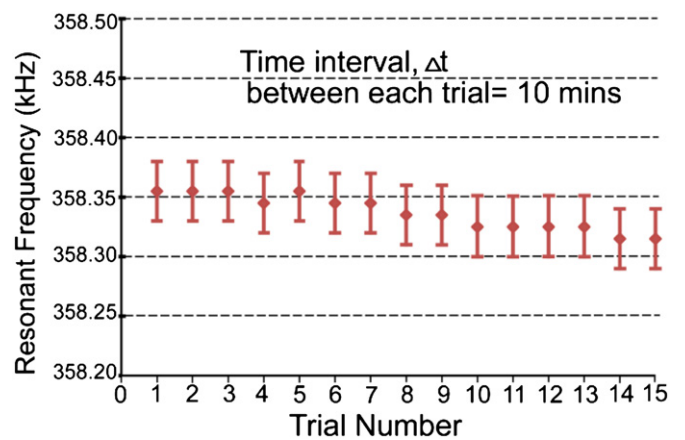

Figure 12. Repeatability assessment for stent cell resonators.

The sensors were characterized for sensitivity to mass loading using paraffin wax to simulate the plaque/tissue depositions. The unloaded sensors were found to have an average weight of 8.5 mg. Mass loads upto 15% of the unloaded mass of the sensor were evaluated. A typical measured resonance response after mass loading is shown in figure 5. Also shown in this figure is the theoretically expected decrease in resonant frequency, assuming uniform mass loading on the sensor.

The measured sensitivity to mass loading was found to range from 630 00 to 650 00 ppm mg^{-1} with a maximum resonant frequency change of 8.1% for 15% mass loading on the sensors. Additionally, the trend observed in measured response agrees with that seen in the theoretical response within 3.5% error.

An assessment of repeatability involved resonance measurements for 15 trials with a time interval of 10 min in between trials with the sensor position and interrogation parameters maintained constant for all trials. The results of the repeatability experiments are detailed in figure 12. The maximum change in resonant frequency measured between trials was around 0.01% or 100 ppm over a time period of 140 min. This corresponds to a mass load of 0.02% of the unloaded sensors mass.

5. Discussion and conclusions

This paper presents the sensor design and evaluation for wireless monitoring of tissue accumulation in stents used to treat PAD. Magenotelastic sensors resonating in their fundamental, longitudinal extensional mode of vibration are integrated to a single stent cell. The Au–In eutectic bonding of sensor material to stent allows for low temperature integration of resonators to stent without affecting its magnetoelastic properties. Benchtop *in vitro* testing of sensors was performed to characterize the sensors for flow velocity, viscosity and mass loading sensitivities.

The FEA simulated resonant frequency of the sensors is within 4.2% of the measured response. The mismatch may be attributed to an error in the assumed material properties or surface irregularities and geometrical imperfections of the tested sensors. A more accurate FEA model taking into account these factors for complex geometries is expected to reduce the mismatch even further.

As a result of the constriction brought about by restenosis, a sensor placed within a stent is subjected to changes in blood flow velocities, viscosity levels and mass accumulation of endothelial cells simultaneously. The sensors should thus be capable of differentiating between these three parameters of interest. We have previously reported how a measurement of quality factor can be used to separate viscosity and mass response for magnetoelastic sensors [7]. However, the sensors should be insensitive to flow velocity for reliable use in this application, which is consistent with the measured results. The sensitivity to viscosity was typically 427 ppm cP^{-1}. The sensors, however, show a large sensitivity to mass loading, with loads as small as 6% of the unloaded sensor mass, producing significant changes in the resonant response. Also, as seen in figure 5, the frequency sensitivity of the sensors has not saturated at the maximum mass load, suggesting that the full scale range of these sensors is even greater than that reached in these tests. A relative assessment of mass loading and viscosity sensitivities favors the use of these sensors as mass detectors in stenosed arteries. However, in the absence of stenosis, these sensors may be used for estimating changes in viscosity as well. This suggests a dual application for these sensors depending on the requirement. Repeatability studies show that the stent cell resonators exhibit a typical, maximum change in unloaded resonant frequency of 0.01% over a period of 140 min. This, in turn, corresponds to a mass load of 0.02% of the unloaded sensor mass, or 1.7 μg for the bi-layer stent cell resonators (which have an average unloaded weight of 8.5 mg). The total drift of the sensors over time is thus negligible in comparison to the mass loading of interest due to restenotic pathologies.

It is to be noted that for this particular application, the measurand of interest includes bio-fouling agents. Stent restenosis occurs due to buildup of 'bio-fouling' endothelial hyperproliferation. The buildup of these 'bio-fouling' agents collectively provides a mass load to the sensors which is interpreted as a resonant shift. These sensors may therefore be used in other applications that are affected by bio-bouling, such as implanted glucose sensors.

The parylene coating used in this work is intended to both reduce the corrosion of the sensor, as well as to provide a surface with improved biocompatibility to the endothelial cells and blood cells. The long term efficacy of parylene in maintaining biocompatibility of the sensor is of interest and should be evaluated in future testing. Other biocompatible coatings such as titanium may be an alternative in this application.

The sensors show a negligible cross sensitivity to flow velocity changes, allowing for reliable measurement of viscosity and mass loading. Although the sensitivity to viscosity is relatively low when compared to that of mass loading, sensors may be operated reliably as viscosity detectors to measure changes between 1.1 and 8.8 cP. As expected, the sensitivity to mass loading ranges from 630 00 to 650 00 ppm mg^{-1}. Although this paper presents the sensors in the context of peripheral artery stents, such devices may be useful for coronary artery diseases as well.

Acknowledgments

References

[1] Ouriel K 2001 Peripheral arterial disease *Lancet* **358** 1257–64
[2] Ouriel K and Zarins C K 1982 Doppler ankle pressure: an evaluation of three methods of expression *Arch. Surg.* **117** 297–300
[3] Ouriel K, Veith F J and Sasahara A A 1988 A comparison of recombinant urokinase with vascular surgery as initial treatment for acute arterial occlusion of the legs *New Engl. J. Med.* **338** 1105–11
[4] Ubbink D T, Tulevski II, Hartog D, Koelemay M J, Legemate D A and Jacobs M J 1997 The value of non-invasive techniques for the assessment of critical limb ischaemia *Eur. J. Vasc. Endovasc. Surg.* **13** 296–300
[5] Visser K and Hunink M G 2000 Peripheral arterial disease: gadolinium-enhanced MR angiography versus color-guided duplex US—a metaanalysis *Radiology* **216** 67–77
[6] Green S R and Gianchandani Y B 2009 Wireless magnetoelastic monitoring of biliary stents *IEEE/ASME J. Microelectromech. Syst.* **18** 64–78
[7] Green S and Gianchandani Y B 2010 Tailored magnetoelastic sensor geometry for advanced functionality in wireless biliary stent monitoring systems *J. Micromech. Microeng.* **20** 075040
[8] Green S, Kwon R, Elta G and Gianchandani Y B 2010 *In situ* and *ex vivo* evaluation of a wireless magnetoelastic bilary stent monitoring system *Biomed. Microdevices* **12** 477–84
[9] Park J Y and Davies J E 2000 Red blood cell and platelet interactions with titanium implant surfaces *Clin. Oral Implants Res.* **11** 530–9
[10] Kouzoudis D and Grimes C A 2000 The frequency response of magnetoelastic sensors to stress and atmospheric pressure *Smart Mater. Struct.* **8** 885–9

[11] Jain M K, Schmidt S, Ong K G, Mungle C and Grimes C A 2000 Magnetoacoustic remote query temperature and humidity sensors *Smart Mater. Struct.* **9** 502–10

[12] Jain M K, Cai Q Y and Grimes C A 2001 A wireless micro-sensor for simultaneous measurement of pH, temperature, and pressure *Smart Mater. Struct.* **10** 347–53

[13] Grimes C A, Kouzoudis D and Mungle C 2000 Simultaneous measurement of liquid density and viscosity using remote query magnetoelastic sensors *Rev. Sci. Instrum.* **71** 3822–4

[14] Grimes C A, Mungle C, Zeng K, Jain M K, Dreschel W R, Paulose M and Ong K G 2002 Wireless magnetoelastic resonance sensors: a critical review *Sensors* **2** 294–313

[15] Cai Q Y and Grimes C A 2000 A remote query magnetoelastic pH sensor *Sensors Actuators* B **71** 112–7

[16] Hernando A, Vazquez M and Barandiaran M 1988 Metallic glasses and sensing applications *J. Phys. E* **21** 1129–39

[17] Modzelewski C, Savage H T, Kabacoff L T and Clark A E 1981 Magnetomechanical coupling and permeability in transversely annealed Metglas 2605 alloys *IEEE Trans. Magn.* **17** 2837–9

[18] O'Handley R C 2000 *Modern Magnetic Materials: Principles and Applications* (New York: Wiley)

[19] Brouha M and van der Borst J 1979 The effect of annealing conditions on the magnetomechanical properties of Fe–B–Si amorphous ribbons *J. Appl. Phys* **50** 7594–6

[20] Soyka V, Kraus L, Zaveta K and Jurek K 1999 Magnetoelastic properties of stress/field annealed $Fe_{80}Cr_2B_{14}Si_{14}$ amorphous alloy *J. Magn. Magn. Mater.* **196–197** 262–3

[21] Clark A and Wun-Fogle M 1989 A new method of magnetostrictivity and magnetostriction measurement *IEEE Trans. Magn.* **25** 3611–3

[22] Kim M H, Lee K S and Lim S H 1999 Magnetostriction measurements of metallic glass ribbon by fiber-optic Mach–Zehnder interferometry *J. Magn. Magn. Mater.* **191** 107–12

[23] Zhai J, Dong S, Xing Z, Li J and Viehland D 2006 Giant magnetoelectric effect in Metglas/polyvinylidene-fluoride laminates *Appl. Phys. Lett.* **89** 083507

[24] Anderson P III 1982 Magnetomechanical coupling, ΔE effect, and permeability in FeSiB and FeNiMoB alloys *J. Appl. Phys.* **53** 8101–3

[25] Modzelewski C, Savage H, Kabacoff L and Clark A 1981 Magnetomechanical coupling and permeability in transversely annealed Metglas 2605 alloys *IEEE Trans. Magn. Mag* **17** 2837–9

[26] ASM International Handbook Committee 1990 *Metals Handbook* (Bilthoven, The Netherlands: ASM Int.)

[27] Lin J J and Perng T P 1995 Embrittlement of amorphous $Fe_{40}Ni_{38}Mo_4B_{18}$ alloy by electrolytic hydrogen *Metall. Mater. Trans.* A **26** 197–201

[28] Lee C C, Wang C Y and Matijasevic G 1993 Au–In bonding below the eutectic temperature *IEEE Trans. Compon. Hybrids Manuf. Technol.* **16** 311–6

[29] Aktakka E E, Kim H and Najafi K 2009 Wafer level fabrication of high performance MEMS using bonded and thinned bulk piezoelectric substrates *IEEE Int. Conf. on Solid State Sensors, Actuators, and Microsystems (Transducers)* 849–52

[30] Sabatier M J, Stoner L, Reifenberger M and McCully K 2006 Doppler ultrasound assessment of posterior tibial artery size in humans *J. Clin. Ultrasound* **34** 223–30

[31] Fronek A, Coel M and Bernstein E F 1976 Quantitative ultrasonographic studies of lower extremity flow velocities in health and disease *Circulation* **53** 957–60

[32] Haynes W M (ed) 2011 *CRC Handbook of Chemistry and Physics* 92nd edn (Boca Raton, FL: CRC Press)